HHS Public Access

Author manuscript

Mol Cancer Ther. Author manuscript; available in PMC 2022 August 01.

Published in final edited form as:

Mol Cancer Ther. 2021 August ; 20(8): 1388–1399. doi:10.1158/1535-7163.MCT-20-0591.

CSF-1/CSF-1R Signaling Inhibitor Pexidartinib (PLX3397) Reprograms Tumor-Associated Macrophages and Stimulates T-cell Infiltration in Sarcoma Microenvironment

Tomohiro Fujiwara, MD, PhD[1,2,3], **Mohamed Yakoub, MD**[1,2], **Andrew Chandler**[1,2], **Alexander Christ, MD**[1,2], **Guangli Yang, PhD**[4], **Ouathek Ouerfelli, PhD**[4], **Vinagolu K. Rajasekhar, PhD**[1], **Yildirim Dogan, PhD**[5,6], **Malcom A.S. Moore, PhD**[5], **Toshifumi Ozaki, MD, PhD**[3], **Ed Purdue, PhD**[2], **John H. Healey, MD, FACS**[1,2]

[1]Department of Surgery, Orthopaedic Service, Memorial Sloan Kettering Cancer Center, 1275 York Avenue, New York, NY 10065, USA

[2]Hospital for Special Surgery, 541 East 71st Street, New York, NY 10065, USA

[3]Department of Orthopaedic Surgery, Okayama University Graduate School of Medicine, Dentistry, and Pharmaceutical Sciences, 2-5-1, Shikata-cho, Kita-ku, Okayama 700-8558, Japan

[4]Organic Synthesis Core Laboratory, Memorial Sloan-Kettering Cancer Center, 1275 York Avenue, New York, NY 10021, USA.

[5]Cell Biology, Memorial Sloan-Kettering Cancer Center, 1275 York Avenue, New York, NY 10021, USA.

[6]AVROBIO Inc., One Kendall Square, Bldg 300, #201, Cambridge, MA 02139. USA.

Abstract

Colony-stimulating factor 1 (CSF-1) is a primary regulator of the survival, proliferation, and differentiation of monocyte/macrophage that sustains the pro-tumorigenic functions of tumor-associated macrophage (TAM). Most targeted therapies against bone and soft-tissue sarcomas have shown little progress towards better prognosis. Here, we investigated the effect of potent inhibitor of CSF-1 receptor (CSF-1R) PLX3397 (pexidartinib), recently approved by the Food and Drug Administration (FDA) for tenosynovial giant-cell tumor, to reprogram TAMs whose

*Corresponding Author: John H. Healey, MD, FACS, Orthopaedic Service, Department of Surgery Memorial Sloan Kettering Cancer Center, 1275 York Ave, New York, NY 10065 USA, Phone: (212) 639-7610 / Fax: (212) 794-4015, healeyj@mskcc.org.

AUTHOR CONTRIBUTIONS

Conception and design: T. Fujiwara, E. Purdue, J.H. Healey

Development of methodology: T. Fujiwara, M. Yakoub, A. Chandler, A. Christ, E. Purdue

Acquisition of data (provided animals, acquired and managed patients, provided facilities, etc.): T. Fujiwara, Y. Mohamed, A. Chandler, A. Christ

Analysis and interpretation of data (e.g., statistical analysis, biostatistics, computational analysis): T. Fujiwara, Y. Mohamed, A. Chandler, A. Christ, E. Purdue, J.H. Healey

Writing, review, and/or revision of the manuscript: T. Fujiwara, O. Ouerfelli, V.K. Rajasekhar, E. Purdue, J.H. Healey

Administrative, technical, or material support (i.e., reporting or organizing data, constructing lentiviral vectors, and databases): A. Christ, O. Ouerfelli, G. Yang, V.K. Rajasekhar, M.A.S. Moore, Y. Dogan, T. Ozaki, E. Purdue, J.H. Healey

Study supervision: J.H. Healey

CONFLICT OF INTEREST

The authors TF, MY, AC1 AC2, GY, OO, RV, TO, EP disclosed no potential conflicts relevant to this article. JH is a paid consultant for Daiichi Sankyo.

infiltration correlates with unfavorable prognosis of sarcomas. First, we confirmed by cytokine arrays of tumor-conditioned media (TCM) that cytokines including CSF-1 are secreted from LM8 osteosarcoma cells and NFSa fibrosarcoma cells. The TCM, like CSF-1, stimulated ERK1/2 phosphorylation in bone marrow-derived macrophages (BMDMs), polarized BMDMs toward a M2 (TAM-like) phenotype, and strikingly promoted BMDM chemotaxis. *In vitro* administration of PLX3397 suppressed pERK1/2 stimulation by CSF-1 or TCM, and reduced M2 polarization, survival, and chemotaxis in BMDMs. Systemic administration of PLX3397 to the osteosarcoma orthotopic xenograft model significantly suppressed the primary tumor growth and lung metastasis, and thus improved metastasis-free survival. PLX3397 treatment concurrently depleted TAMs and $FOXP3^+$ regulatory T cells and, surprisingly, enhanced infiltration of $CD8^+$ T cells into the microenvironments of both primary and metastatic osteosarcoma sites. Our preclinical results show that PLX3397 has strong macrophage- and T cell-modulating effects that may translate into cancer immunotherapy for bone and soft tissue sarcomas.

Keywords

Sarcoma; Tumor-associated macrophage; CSF-1R; Immunotherapy

INTRODUCTION

Tumor-associated macrophage (TAMs) represent a substantial proportion of all tumor-infiltrating immune cells in the tumor microenvironment (TME), have a dominant role as orchestrators of tumor-related inflammation toward tumor growth and progression, and are potential new therapeutic targets (1,2). The tumor-promoting function of TAMs is based on their ability to secrete proangiogenic and growth factors, as well as to potently suppress T cell effector function by releasing immunosuppressive cytokines (1,3,4). Two opposing phenotypes, termed classically activated (or M1-like) and alternatively activated (or M2-like), have been associated with anti- and protumoral functions (1,2). Clinically, M2-like TAMs are associated with high tumor grade and poor prognosis in many carcinomas and sarcomas (1,2,5). TAM-targeting treatment strategies are under early phase investigation in various cancer types, but not in sarcoma, although trans-differentiating M2-like macrophages to M1-like macrophages has great potential as a new sarcoma therapy.

Despite major advances in multimodality therapies for sarcomas, more than one-third of patients show a poor response to conventional therapy, resulting in subsequent recurrence and a poor1 prognosis (6,7). The overall survival for osteosarcoma is 60%–70% at five years (8), but less than 30% for patients who present with metastatic disease (6). Similarly, the median overall survival is around one year for metastatic soft-tissue sarcoma (9), and approximately 10% of patients are alive at five years (10,11), highlighting the need for innovative drugs or approaches.

Colony-stimulating factor 1 (CSF-1) plays a significant role in the recruitment of peripheral blood monocytes to the TME, differentiation into macrophages, and polarization of macrophages towards an M2-like phenotype via binding to the CSF-1 receptor (CSF-1R) (12). Preclinical studies have shown that CSF-1R blockade may inhibit tumor growth in

several cancer models through the elimination or repolarization of TAMs (13,14). PLX3397 (pexidartinib), a potent CSF-1R inhibitor, has been shown to be effective for tenosynovial giant cell tumor (TGCT), which express CSF-1 (15,16), and was recently approved by the US Food and Drug Administration (FDA) for symptomatic TGCT (17). While several preclinical and clinical trials have been ongoing for several malignant tumors (16,18,19), evidence of PLX3397 in sarcomas is limited (20).

In this study, we investigated the efficacy and safety of PLX3397 in our established *in vitro* and *in vivo* sarcoma TAM model. We demonstrate that CSF-1/CSF-1R blockade using PLX3397 suppresses survival, migration, and M2 poralization of sarcoma TAMs *in vitro* and significantly inhibits osteosarcoma growth and metastatic spread *in vivo*. Furthermore, we found that PLX3397 administration resulted in not only depleting TAMs but also altering T cell infiltration in the tumor microenvironment. This preclinical trial demonstrates that PLX3397 is a promising immunotherapeutic agent and would have immediate clinical implications for sarcomas, which should be explored for further clinical development.

MATERIALS AND METHODS

Cell lines and cell culture

The murine osteosarcoma cell line LM8 (RCB1450) and the murine fibrosarcoma cell line NFSa (RCB0282) were purchased from the Riken Cell Bank (Tsukuba, Japan). These cell lines have C3H mouse origin, and the LM8 cell line, a highly metastatic cell line, was derived from Dunn's osteosarcoma (21). LM8 clones expressing the luciferase and tdTomato, named *LM8-Luc*, were generated with a lentiviral vector (Supplementary Methods and Supplementary Fig. S1). These cell lines were maintained in Dulbecco's modified Eagle's medium (DMEM; Life Technologies, Inc., Grand Island, NY), containing 10% heat-inactivated fetal bovine serum (FBS) (Life Technologies) , 1% penicillin (100 U/mL), and streptomycin (100 mg/mL; Life Technologies). The cells were maintained under 5% CO_2 in a humidified incubator at 37° C.

Preparation of tumor-conditioned media (TCM)

LM8 and NFSa cells were seeded at 1×10^7 cells per T175 cell culture flask in 30 μl of DMEM containing 10% FBS and 1% penicillin and streptomycin. After 48 hours, supernatant was collected, passed through a 0.2 μm vacuum filter (VMR, Randor, PA), and stored at −20° C.

Cytokine array

Cytokine array analysis was performed using 500 μl of freshly stored TCM and the Mouse Cyokine Array panel A (R&D Systems Minneapolis, MN), according to the manufacture's protocol.

Preparation of bone marrow-derived macrophages (BMDMs)

Bone marrow cells were isolated and harvested from the femur, tibia, and humeri of 6–8 week-old C3H/HeJ female mice (Jackson laboratories, Bar Harbor, ME), as previously described (22) with the Hospital for Special Surgery's (HSS's) Institutional Animal

Care and Use Committee (IACUC) approved protocol (#2016-0039). Bone marrow cells were differentiated into BMDMs with α-Minimum Essential Medium (α-MEM; Life Technologies) supplemented in 10% FBS, 1% penicillin and streptomycin, and 10% (equivalent to 140 ng/ml CSF-1) conditioned media from the CSF-1 over-producing cell line CMG (22,23) or TCM from cultured LM8 or NFSa for five days until confluent.

PLX3397 treatment *in vitro* and *in vivo*

The CSF-1R inhibitor PLX3397 was purchased (Bioactive Molecular Research, FL), and its analytical profile was further confirmed in our laboratory and compared to previously reported data (15). For *in vitro* studies, a 10 mmol/l (mM) stock of PLX3397 was formulated in dimethyl sulfoxide (DMSO), which was used as the vehicle control. For *in vivo* studies, PLX3397 was formulated in 20% DMSO at a concentration of 5 mg/kg and 10 mg/kg.

Animal model

All animal studies were approved by HSS's IACUC (#2016-0039). Six- to eight-week old female C3H/HeJ mice (Jackson Laboratory; Bar Harbor, ME) were anesthetized by exposure to 3% isoflurane on Day zero and subsequent days. On Day zero, the mice were anesthetized with 3% isoflurane, and the right leg was disinfected with 70% ethanol. A 100 μL volume of solution containing 1×10^6 LM8-Luc cells was orthotopically injected into the proximal tibia (24).

Evaluation of PLX3397 administration in mice with spontaneous lung metastases of osteosarcoma

Individual mice were retro-orbitally injected with 100 μl of PLX3397 (5 mg/kg or 10 mg/kg) or control phosphate-buffered saline (PBS) per injection on Days seven and 14 post-inoculation of LM8-Luc cells. Each experimental condition included five animals per group. Photons from firefly luciferase were counted using the IVIS imaging system (Xenogen, Alameda, CA) following intraperitoneal injection of d-luciferin (150mg/kg; Promega). Following the evaluation of the primary sites, chest lesions of mice were analyzed individually if the spill/leakage of photons from the primary sites were suspected. Data were analyzed using LivingImage software (version 4.7.2; Xenogen). On Day 21, the end of the experiment, the primary tumor and lung of each animal were resected at necropsy for histological analysis. A blood examination, weighing of each mouse body, and a histological examination of the liver were performed for drug toxicity assessment.

Immunohistochemistry

All tumors resected from mouse primary tumors and lungs were fixed with 10% buffered formalin before paraffin embedding. A rabbit polyclonal anti-CD68 antibody (Boster; Pleasanton, CA; cat#PA1518), a rabbit monoclonal anti-CD8 antibody (Cell Signaling Technology, MA; cat#98941), and a rat monoclonal anti-FOXP3 (eBioscience; cat#14-5773-82) were used in concentrations of 5 μg/ml, 4.8 μg/ml, and 5 μg/ml, respectively. The tissue sections were blocked for 30 minutes in 10% normal goat serum, 2% bovine serum albumin in PBS. A five-hour incubation with the primary antibody was followed by a 32-minute incubation with biotinylated goat anti-rabbit IgG (1:200 dilution;

Vector Laboratories; cat#PK4001). Sequential incubations were performed with Secondary Antibody Blocker, Blocker D, Streptavidin-HRP and Tyramide Alexa Fluor 488 (Life Technology; cat#B40932). Histology slides were digitally scanned with Pannoramic Flash (3DHistech; Budapest, Hungary) using 20x/0.8NA objective. Snapshots were taken using CaseViewer Software (3DHistech).

Statistical analysis

All statistical analyses were performed using Prism (GraphPad Prism version 5; San Diego, CA, USA) or SPSS Statistics version 24 (IBM, Armonk, NY, USA). The unpaired t test or one-way ANOVA, corrected for multiple comparisons as appropriate, was used to determine the significance of any differences between experimental groups. Results were shown as means ±SEM or ±SD as indicated. The Kaplan-Meier method and the log-rank test were used to analyze metastasis-free survival. Metastasis-free survival was defined as the time interval from tumor inoculation until initial metastasis detected by IVIS imaging. The value of $p < 0.05$ was considered to be statistically significant.

Additional details are in the Supplementary Merthods.

RESULTS

Characterization of osteosarcoma and fibrosarcoma secretory profiles of chemokines/cytokines

In order to establish an *in vitro* TAM model of sarcomas, we differentiated bone marrow cells in the presence of TCM from the CSF-1 overproducing cell line CMG (23,25) and TCM from osteosarcoma LM8 cells and fibrosarcoma NFSa cells. To comprehensively profile production of cytokines/chemokines (including CSF-1) from CMG, LM8, and NFSa, we performed cytokine array analysis using conditioned media (CM) from these cells. We found striking differences among the cytokine/chemokine profiles of CMG, LM8, and NFSa CM (Fig. 1A). CSF-1 production was observed in all these CM; the highest production was identified from LM8, followed by NFSa and CMG (Fig. 1B). Various other cytokines/chemokines, including interferon (IFN)-γ, chemokine (CXC) ligand (CXCL)-1, chemokine (CC motif) ligand (CCL)-2, CCL-5, CXCL-12, and tissue inhibitor of the metalloproteinase (TIMP)-1 were also produced from CMG (Fig. 1A-1B). However, most of these, except for IFN-γ and TIMP-1, were more highly produced by LM8 and NFSa compared to CMG (Fig. 1B). We also identified differences in production levels of cytokines/chemokines including IFN-γ-Inducible Protein (IP)-10, CXCL-1, CCL-2, CXCL-9, CXCL-2, and CXCL-12 between LM8 and NFSa (Fig. 1B). Based on these results, we hypothesized CM from the three cell lines would have distinct and differential effects on proliferation and polarization of macrophages.

Establishment of in vitro model of tumor-associated macrophage produced by sarcoma cell conditioned media

Mouse BMDMs were obtained by flushing the long bones of C3H/HeJ mice, a host strain of LM8 and NFSa cells, and were expanded in culture supplemented with CM from CMG, LM8, and NFSa cells. Morphologically, these cells had a spindle-shaped, fibroblast

appearance after expansion, which are slightly different among BMDM-CSF-1, BMDM-LM8, and BMDM-NFSa for both length and number of the dendritic extension (Fig. 2A). Macrophage differentiation and polarization are induced with increased mitogen-activated protein kinase (MAPK)/extracellular signal-regulated kinase (ERK) pathway, characterized by the activation of ERK1/2 (26). When pure murine M-CSF (50 ng/mL) was added to the BMDMs, enhanced phosphorylated ERK1/2 (pERK1/2) was detected with a peak stimulation after five minutes of treatment (Fig. 2B). Similarly, enhanced pERK1/2 was also detected when TCM/LM8 and TCM/NFSa were added to BMDMs at a 50/50 ratio with culture media (Fig. 2B).

In order to investigate the polarization of BMDMs toward an M2/TAM-like phenotype, we compared surface marker profiles by flow cytometry and gene expression profiles related to M1- and M2-like phenotypes. Flow cytometry analysis revealed BMDM/CSF-1 had a high frequency (94%) of positivity for the M2 marker CD206, indicating polarization towards an M2-like phenotype (Fig. 2C). Yet, BMDM-LM8 and BMDM-NFSa had slightly more heterogeneous population with 64% and 71% $CD206^+$ within $CD45^+/CD11b^+$ populations, respectively (Fig. 2C). However, the mean fluorescence intensity (MFI) of $CD206^+/CD80^+$ showed no significant difference among BMDM-CSF-1, BMDM-LM8, and BMDM-NFSa (Fig. 2C), indicating all of these BMDMs polarized toward M2-like phenotype. Reverse transcription quantitative-PCR (RT-qPCR) analysis revealed BMDM-TCM/LM8 and BMDM-TCM/NFSa had higher mRNA expression of M1-like genes, including *IL-1β*, *iNOS*, and *CD80* (Supplementary Fig. S2) than BMDM-CSF-1, which could be attributed to the GM-CSF secreted from LM8 and NFSa cells (Fig. 1B). Yet, BMDM-TCM/NFSa showed greater mRNA expression of M2-like genes, including *CD206* and *CCL-2*, than BMDM-CSF-1 (Supplementary Fig. S1B). These data confirmed TCM/LM8 and TCM/NFSa were able to polarize BMDMs into an M2-like phenotype, while CSF-1/CMG differentiated BMDMs toward a pure M2-like phenotype.

Malignant tumors have a major role in recruitment of circulating monocytes and macrophages into the TME (1,2). Therefore, we investigated whether BMDMs were recruited under stimulation of CSF-1/CMG, TCM/LM8, and TCM/NFSa by transwell assays. BMDMs were able to migrate through the transwell chamber with 8 μm pores in response to CSF-1/CMG, TCM/LM8, and TCM/NFSa (Fig. 2D). Notably, the chemotaxis of BMDMs was enhanced by 1.5 to 2-fold change in response to TCM/LM8 and TCM/NFSa as compared to CSF-1/CMG (Fig. 2D). These results indicate CSF-1/CMG, TCM/LM8, and TCM/NFSa can recruit macrophages, where TCM/LM8 and TCM/NFSa were more effective than CSF-1/CMG.

PLX3397-dependent CSF-1R inhibition is sensitive to M2-like polarization, cellular viability, and chemotaxis of tumor-associated macrophages produced by sarcoma cells

Survival and polarization of macrophares are dependent on CSF-1R signaling (5). To validate this contention and also gain further molecular insight in this process, we exploited the PLX3397, a potent inhibitor of CSF-1R signaling. The PLX3397, at the given doses 50 nM, 100 nM, and 250 nM strongly inhibited the ERK activity as measured by

phosphorypated ERK1/2 levels in Western blots, which was otherwise stimulated at 10 minutes of exposure to M-CSF, TCM/LM8, and TCM/NFSa (Fig. 3A).

Next, we tested if CSF-1R inhibition had an effect on macrophage polarization using flow cytometry analysis and RT-qPCR. Flow cytometry data revealed the PLX3397 dose-dependently decreased in the measurable populations of $CD45^+/CD11b^+/CD206^+$ cells in BMDM-CSF-1, BMDM-LM8, and BMDM-NFSa (Fig. 3B and Supplementary Fig. S1C). Additionally, the MFI of $CD206^+/CD80^+$ decreased in all of these cells more than 50% at 500 nM PLX3397 relative to the control cells (Fig. 3B). The most significant effect was observed in BMDM-LM8, where $CD206^+/CD80^-$ population (M2-like phenotype) shifted from 95% in untreated BMDM-LM8 to 60% in BMDM-LM8 treated with 500 nM PLX3397. There was a 65% of decrease in $CD206^+/CD80^+$ MFI. (Fig. 3B). Furthermore, the RT-qPCR analysis for M1 and M2 genes revealed PLX3397 also reduced the expression levels of M2 genes, including *CD206* and *CCL-2,* in a dose dependent manner (Fig. 3C). Yet, the expression levels of M1 genes including *IL-1β*, *iNOS*, and *CD80* were dose dependently enhanced by PLX3397 (Fig. 3C). These data suggest CSF-1R inhibition induces gene expression changes in TAMs and reduces M2 macrophage polarization in bone and soft-tissue sarcoma models.

In order to evaluate how CSF-1R inhibition affect survival of TAMs, we investigated cellular viability with increasing dose of PLX3397. After PLX3397 treatment for 24 hours, we also observed significantly reduced cellular viability in a dose dependent manner (Fig. 3D). The effect on macrophage viability was most striking in BMDM-CSF-1 (Fig. 3D). Next, we tested whether CSF-1R inhibition also affects chemotaxis of TAMs, which was enhanced by CSF-1/CMG, TCM/LM8, and TCM/NFSa (Fig. 2E). After PLX3397 treatment for one hour, the cellular chemotaxis of BMDM-TAMs through the trans-well membrane was significantly reduced in a dose-dependent manner (Fig. 3E). Collectively, these data indicated CSF-1R inhibition results in reduced survival and migration of TAMs, which prompted testing the efficacy of PLX3397 with a potential preclinical value on development of sarcoma and its metastasis.

PLX3397-depedent CSF-1R inhibition blocks the progression of osteosarcoma and improves metastasis-free survival

In order to perform preclinical testing of PLX3397, we first determined the ability of LM8 cells infected with lentiviral vector expressing firefly luciferase to monitor the development of primary tumor at the orthotopic site and subsequently its spontaneous metastasis to lung in the C3H/HeJ mice (21). We transplanted 1.0×10^6 LM8-luc cells into the right proximal tibia. The mice were analyzed for tumor growth by following the increase in luciferase bioluminescence measured in the IVIS imager. Similarly, we also visualized the onset and growth of distant metastases such as in lung. Five days after the orthotopic transplantation of the tumor cells, primary tumors were macroscopically detectable in all mice, but no signals were detected in the lungs (Supplementary Fig. S2A). At Day 12 post-tumor cell transplantation, the first detectable metastasis in some of the mice by IVIS was observed (Supplementary Fig. S2B). By Day 19 post tumor cell transplantation, all animals showed signals in their lungs by IVIS (Supplementary Fig. S2C). By the end of three

weeks following the initial tumor cell transplantation, lung metastases become detectable by luciferase imaging and also verified by the bioluminance of luciferase in the excised lungs following the necropsy of the mice. We also histologically verified the metastases foci in the excised lungs by hematoxylin and eosin (H&E) staining. (Supplementary Fig. S2D).

Next, we investigated the therapeutic effect of PLX3397 on the primary and spontaneous lung metastasis of osteosarcoma. Tumor bearing-mice were administered retro-orbitally with two therapeutic doses, 5 mg/kg (low-dose group), or 10 mg/kg (high-dose group) of PLX3397 by maintaining the control group with PBS injection. All the treatments into mice in each group ($n = 5$) were administered twice; one at seven days and the other at 14 days after the orthotopic transplantation of the LM8-luc cells. Tumor size was monitored weekly, which revealed tumor growth was significantly suppressed by administration of high-dose PLX3397 compared with low-dose PLX3397 or PBS (Fig. 4A). High-dose PLX3397-treated mice had the tumors were consistently smaller than those treated with low-dose PLX3397 or PBS-treated tumors, when measured on Day 19 after tumor cell transplantation (Fig. 4B). The development of a primary tumor and lung metastasis were again monitored weekly. At the end of week one, firefly luciferase activity was detected at the primary lesion in each group (Supplementary Fig. S3A). At Day 12, one mouse (20%) in the control group showed a signal presumptively in the lung (pulmonary area), suggesting metastasis into the lung. However, no signal was detected in the lung in the PLX3397-treated groups (Supplementary Fig. S3B). At Day 19, luciferase activity in the high-dose PLX3397 group were significantly weaker than those in the low-dose PLX3397 group and control group (Fig. 4C-D). Similarly, none of the mice in the high-dose PLX3397 group showed the metastatic signal in the lung (100% inhibition), compared to four mice (20% inhibition) in the control group and three mice (40% inhibition) in the low-dose PLX3397 group (Fig. 4E and Supplementary Fig. S3C). The presence of metastases in the resected lung was also confirmed after all mice were euthanized at the end of three weeks (Day 22) post necropsy bioluminance and immunohistochemistry. All mice in the control group and low-dose PLX3397 group showed signals from the resected lung, whereas low intensity signals were detected in three mice (60%) in the high-dose PLX3397 group (Supplementary Fig. 3D). Both the number and size of lung metastases were validated by histopathological examination. We observed smallest number and size of metastatic osteosarcoma in the lungs of high-dose PLX3397-treated mice compared to those of low-dose PLX3397 or PBS-treated mice (Fig. 4F). Based on these results, we evaluated metastasis-free survival, which revealed high-dose PLX3397-treated mice showed longest metastasis-free survival periods among the three groups in Kaplan-Meier analysis (log-rank test, $p = 0.0137$; Fig. 4G).

No apparent systemic effects and weight loss were identified following drug administrations (Supplementary Fig. S4A). In light of the hepatotoxicity and renal toxicity reported in the human use of this drug, we also evaluated liver and renal toxicity at baseline and on Day 22, measuring aspartate aminotransferase (AST), alanine aminotransferase (ALT), and creatinine (CREA). We observed non-statistically significant increases in AST and ALT levels in two of five mice (40%) treated with high-dose PLX3397 (Supplementary Fig. S4B – 4C). The histopathological examination of the liver revealed no evidence of necrosis, fibrosis, steatosis, inflammation, or biliary changes in any of the three groups (Supplementary Fig. S5). The levels of lactate dehydrogenase, alkaline phosphatase, total

bilirubin, total protein, albumin, cholesterol, and creatinine levels did not show any significant variations among the treatment groups (Supplementary Fig. S4D – S4J).

PLX3397 treatment results in depletion of TAMs and alters T cell composition in the TME

To understand how CSR-1R inhibition elicited a potent anti-tumor response *in vivo*, we performed flow-cytometric analysis using the dissociated tumor cells from the PLX3397-treated mice by maintiang the PBS-treated set as a parallel control. We observed significantly decreased density of dTomato$^+$ cells in the tumors of high-dose PLX3397-treated mice, indicating an altered composition of tumor cells versus the cells of TME (Fig. 5A and Supplementary Fig. S6A). Contrarily, tumor infiltrating CD45$^+$ myeloid cells were significantly increased in the tumors of high-dose PLX3397-treated mice compared to thouse of PBS-treated tumors (Fig. 5A and Supplementary Fig. S6A). Under the same experimental conditions, we observed significantly decreased CD45$^+$CD11b$^+$ macrophages in the PLX3397-treated tumors (Fig. 5A and Supplementary Fig. S6A). In a comparison of M1- and M2-like phenotypes between treatment groups, the accumulation of both CD45$^+$CD11b$^+$CD206$^+$ M2-like phenotype and CD45$^+$CD11b$^+$CD80$^+$ M1-like phenotype was decreased with the PLX3397-treatment (Fig. 5A, 5B and Supplementary Fig. S6A). However, the MFI of CD45$^+$CD11b$^+$CD206$^+$/CD45$^+$CD11b$^+$CD80$^+$ was significantly decreased in the high-dose PLX3397-treated tumors (Fig. 5A), indicating the systemic administration of 10mg/kg of PLX3397 resulted in a polarization of TAMs against the M2-like phenotype.

CSF-1R inhibition alters the TME composition of other immune cells (3,4). We also investigated the comparative levels of other immune cell types in osteosarcoma tumors by flow cytometry. While the accumulation of CD45$^+$CD3$^+$ T lymphocytes remained same between treated versus the control (Fig. 5C and Supplementary Fig. S6B), there was an increased subpopulation of CD8$^+$ T cells in high-dose PLX3397-treated tumors (Fig. 5B and 5C). Yet, the accumulation of CD4$^+$ T cells remain unaltered (Fig. 5C and Supplementary Fig. S6B). Similarly, we also observed the unchanged quantity of CD45$^+$CD19$^+$ B cells among the treatment groups (Fig. 5C and Supplementary Fig. S6B. There was a decreased number of CD68$^+$ macrophages (Fig. 5E and Supplementary Fig. S7) in the high-dose PLX3397-treated tumors. Conversely, we observed an increased CD8$^+$ T cells in the high-dose PLX3397-treated tumors (Fig. 5E and Supplementary Fig. S7). Additionally, the number of FOXP3$^+$ regulatory T cells was significantly decreased in the high-dose PLX3397-treated tumors (Fig. 5D, 5E and Supplementary Fig. S7). These findings in all of the above cell types were observed in osteosarcoma microenvironment at both primary (Fig. 5E) and metastatic sites (Supplementary Fig. S7). Our results showed systemic administration of PLX3397 reduced the infiltrating TAMs, with a shift from the M2-like to M1-like phenotype. At the same experimental therapeutic conditions, the CD8$^+$ T cell numbers were preferentially increased over the decreasing levels of FOXP3$^+$ T cells.

DISCUSSION

We describe the preclinical evidence of the efficacy of PLX3397, a potent CSF-1R inhibitor, in a sarcoma model. PLX3397 inhibited M2 polarization, cellular proliferation,

and chemotaxis of macrophages in our established *in vitro* sarcoma TAM models. The antitumor effect of PLX3397 was confirmed in the preclinical model using osteosarcoma-bearing mice. These findings are the first delineation of the role of a small molecule (PLX3397) in modulating the sarcoma microenvironment of primary and metastatic sites, and retarding osteosarcoma progression.

PLX3397 is a small molecule designed to block the CSF-1 receptor with restricted kinome targets approved for the treatment of adult patients with symptomatic TGCT (16,17). Preclinical tests demonstrated the antitumor effect of PLX3397 in mice with lung, breast, and prostate cancer, melanoma, and gastrointestinal stromal tumor (GIST) (14,27). PLX3397 is also being investigated to treat various malignancies, either as monotherapy or in combination with other drugs, for glioblastoma, melanoma, and metastatic breast cancer (17). Furthermore, PLX3397 enhanced the efficacy of chemotherapy (28,29) or radiotherapy (14,30) in breast or prostate cancer, respectively. The interaction of this therapy with the immune system is suggested in a phase I dose escalation study of PLX-3397, among various advanced cancer histologies in which markedly reduced subsets of circulating monocytes ($CD14^{dim}/CD16^{+}$) were found (31). Preliminary data from a phase 1 study combined cabiralizumab (anti CSF-1R) and anti-PD-1 mABs reported found a response in 4/31 (13%) of advanced pancreas cancer patients (32,33). The prevalence of TAMs in osteosarcoma and correlation with poor outcome suggests that CSF-1R inhibitors like PLX3397 are promising agents for clinical development with immunomodulators in patients with this orphan disease.

We identified striking differences in cytokine secretion from distinct sarcoma tumor cell lines, including CSF-1, CCL-2, CCL-5, IP-10, CXCL-1, CXCL-2, and CXCL-12 *in vitro*. These differences likely underlie the variations in response to PLX3397 among macrophage populations differentiated in the presence of TCM from these sarcoma cells. For example, BMDMs chemotaxis in response to TCM/LM8 and TCM/NFSa was remarkably enhanced compared to pure CSF-1. These results indicated cytokines/chemokines other than CSF-1 in TCM/LM8 and TCM/NFSa can also promote macrophage recruitment. Evidence suggests CCL2, overexpressed in a wide range of tumors, is involved in recruitment of macrophage and lack of CCL2 signaling reduces macrophage infiltration (34). CXCL-1 is also known to recruit macrophages into the TME (35). The presence of these chemokines may explain the residual BMDMs infiltrating through membrane even in the presence of PLX3397 (Fig. 3E). Notably, studies suggest the chemotaxis of M1 and M2 macrophages is fine-tuned by different chemokines in the process of inflammation associated with tumorigenesis (36). Regarding macrophage survival, our findings demonstrated the most striking effect of PLX3397 with the use of pure CSF-1, followed by TCM-LM8 and TCM-NFSa (Fig. 3D). These differences on macrophage viability might be also attributed to the differential expression of cytokines included in the TCM/LM8 and TCM/NFSa. Evidence indicates CCL-2, CCL-3, and CCL-14 stimulate proliferation of TAMs (37). These chemokines also activate normal macrophage polarization and differentiation into TAMs (37), which partially explain the differences in expression of M1 and M2 related markers among BMDM-CSF-1, BMDM-LM8, and BMDM-NFSa (Fig. 2C-2D and Fig. 3B-3C). These data indicated the possible benefit of targeting chemokines in addition to CSF-1R blockade in depleting TAMs for bone and soft-tissue sarcomas.

Notably, the clinical benefits occurred without evidence for significant hepatotoxicity. In the pivotal ENLIVEN trial, treatment-emergent adverse events (TEAEs) resulted in permanent treatment discontinuation in 13% pexidartinib recipients, in who most of these were liver-related (16). TEAEs also led to treatment interruption or dose reduction in 38% pexidartinib recipients. This was most commonly due hepatic adverse events including, AST and ALT increase (16). These findings underscore the necessity of the development of a novel approach to avoid liver toxicity of PLX3397. Recent development of nanomedicine strategies targeting TAMs are encouraging (38) and would be a key to overcome the liver toxicity associated with the systemic administration of PLX3397.

In addition to the depletion of TAMs in our mouse osteosarcoma model, systemic PLX3397 resulted in decreased $FOXP3^+$ regulatory T cells and increased CD8 T lymphocytes within the osteosarcoma microenvironment. A positive-feedback loop between $FOXP3^+$ regulatory T cells and M2 macrophages was recently identified (39). M2-polarized macrophages in the tumor environment promote the differentiation of $CD4^+CD25^-$ T cells into regulatory T cells which, in turn, skew the differentiation of monocytes toward M2 macrophages (39). Thus, the decreased $FOXP3^+$ regulatory T cells *in vivo* can be explained by the depletion of M2-polarized macrophages. The finding regarding the number of CD8 T cells was consistent with recent findings in the preclinical testing for multiple carcinomas (3,4,40), in which CSF-1R blockade led to increased number of CD8 T cell with approximately 1.5 to 5.5–fold change. Similarly, another therapeutic approach targeting TAMs by inhibition of the myeloid PI3K isoform, which induces proinflammatory gene expression in TAMs, showed anti-tumor effect in mouse models of carcinoma and melanoma, by increasing CD8 T cell infiltration without directly affecting T cell activation or cytotoxicity (41). Several mechanisms can be envisioned for the CD8 T cell recruitment after macrophage depletion. First, a change in the adhesive environment, which CD8 T cell encounter in the TME by CSF-1R inhibition, might explain the increased infiltration of CD8 T cell, because macrophages express numerous adhesion molecules for T cells (40). In the inflammatory settings, for example, macrophages are shown to form conjugates with T cells (40). Second, a change of chemokine levels in the TME might explain increased CD8 T cell migration. Evidence suggests increased levels of CCL2, CXCL9, and CXCL10 following CSF-1R inhibition contribute to CD8 T cell trafficking to tumors (4,40,42), although the mechanism underlying the increase of these inflammatory chemokines following the depletion of TAMs remains to be elucidated. Furthermore, recent evidence has shown CSF-1R blockade improve checkpoint immunotherapy by enhancing $CD8^+$ and $CD4^+$ T cell activities (4,40,43). Further preclinical and clinical testing of combination therapy CSF-1R blockade and immune checkpoint inhibitors could be an important step for development of a novel therapeutic strategy for bone and soft-tissue sarcomas.

In summary, we present the antitumor effect of a potent CSF-1R kinase inhibitor, PLX3397, in our established preclinical model of sarcomas. CSF-1R blockade in *in vitro* TAM model resulted in reduced viability and chemotaxis of macrophages and polarization from M2-like to a more M1-like phenotype. Systemic administration of PLX3397 in osteosarcoma model mice suppressed primary tumor growth and spontaneous lung metastasis, improving metastasis-free survival. Additionally, the effects of PLX3397 were not limited to depleting TAMs but also decreased $FOXP3^+$ regulatory T cells and increased CD8 T cell migration

and infiltration into tumors. On the basis of current evidence, PLX3397 would provide a promising immunotherapeutic approach to many cancer types encompaaing carcinoma, melanoma and sarcoma, encouraging the combined use with immune checkpoint blockade therapy in addition to conventional chemotherapy and radiotherapy.

Supplementary Material

Refer to Web version on PubMed Central for supplementary material.

ACKNOWLEDGMENTS

The authors thank Dr. Afsar Barlas and his laboratory members, the MSK Molecular Cytology Core Facility, and the MSK Flow Cytometry Core Facility. We also thank Dr. Umeshkumar K. Bhanot and his laboratory members, the MSK Pathology Core Lab, for pathological evaluation of primary and metastatic tumors and organs in the therapeutic test using animals. We also thank Jessica Massler for her editorial assistance.

Financial support:

The Major Family Fellowship, the Reindeer Run Research Fund, Nanotechnology Center, Memorial Sloan Kettering Cancer Center Project #302 (J.H. Healey)

NCI P30 CA008748-53 Cancer Center Support Grant (Dr. O Ouerfelli)

NCI R50 CA243895-01 (Dr. O. Ouerfelli)

A grant-in-aid for overseas research fellowships from the Yasuda Medical Foundation (2018; T. Fujiwara)

A grant-in-aid for overseas research fellowships from the Japan Society for the Promotion of Science (201860336; T. Fujiwara)

REFERENCES

1. Noy R, Pollard JW. Tumor-associated macrophages: from mechanisms to therapy. Immunity 2014;41(1):49–61 doi 10.1016/j.immuni.2014.06.010. [PubMed: 25035953]
2. Mantovani A, Marchesi F, Malesci A, Laghi L, Allavena P. Tumour-associated macrophages as treatment targets in oncology. Nat Rev Clin Oncol 2017;14(7):399–416 doi 10.1038/nrclinonc.2016.217. [PubMed: 28117416]
3. Ries CH, Cannarile MA, Hoves S, Benz J, Wartha K, Runza V, et al. Targeting tumor-associated macrophages with anti-CSF-1R antibody reveals a strategy for cancer therapy. Cancer Cell 2014;25(6):846–59. [PubMed: 24898549]
4. Zhu Y, Knolhoff BL, Meyer MA, Nywening TM, West BL, Luo J, et al. CSF1/CSF1R blockade reprograms tumor-infiltrating macrophages and improves response to T-cell checkpoint immunotherapy in pancreatic cancer models. Cancer Res 2014;74(18):5057–69 doi 10.1158/0008-5472.CAN-13-3723. [PubMed: 25082815]
5. Pyonteck SM, Akkari L, Schuhmacher AJ, Bowman RL, Sevenich L, Quail DF, et al. CSF-1R inhibition alters macrophage polarization and blocks glioma progression. Nat Med 2013;19(10):1264–72 doi 10.1038/nm.3337. [PubMed: 24056773]
6. Kager L, Zoubek A, Pötschger U, Kastner U, Flege S, Kempf-Bielack B, et al. Primary metastatic osteosarcoma: presentation and outcome of patients treated on neoadjuvant Cooperative Osteosarcoma Study Group protocols. J Clin Oncol 2003;21(10):2011–8. [PubMed: 12743156]
7. Jemal A, Siegel R, Ward E, Hao Y, Xu J, Thun M. Cancer statistics. Ca Cancer J Clin 2009;59(4).
8. Mirabello L, Troisi RJ, Savage SA. Osteosarcoma incidence and survival rates from 1973 to 2004. Cancer 2009;115(7):1531–43. [PubMed: 19197972]
9. Italiano A, Mathoulin-Pelissier S, Cesne AL, Terrier P, Bonvalot S, Collin F, et al. Trends in survival for patients with metastatic soft-tissue sarcoma. Cancer 2011;117(5):1049–54. [PubMed: 20945333]

10. Savina M, Le Cesne A, Blay J-Y, Ray-Coquard I, Mir O, Toulmonde M, et al. Patterns of care and outcomes of patients with METAstatic soft tissue SARComa in a real-life setting: the METASARC observational study. BMC Medicine 2017;15(1):78. [PubMed: 28391775]
11. Tawbi HA, Burgess M, Bolejack V, Van Tine BA, Schuetze SM, Hu J, et al. Pembrolizumab in advanced soft-tissue sarcoma and bone sarcoma (SARC028): a multicentre, two-cohort, single-arm, open-label, phase 2 trial. Lancet Oncol 2017;18(11):1493–501 doi 10.1016/s1470-2045(17)30624-1. [PubMed: 28988646]
12. Hamilton JA. Colony-stimulating factors in inflammation and autoimmunity. Nat Rev Immunol 2008;8(7):533–44 doi 10.1038/nri2356. [PubMed: 18551128]
13. Cuccarese MF, Dubach JM, Pfirschke C, Engblom C, Garris C, Miller MA, et al. Heterogeneity of macrophage infiltration and therapeutic response in lung carcinoma revealed by 3D organ imaging. Nature communications 2017;8(1):1–10.
14. Peyraud F, Cousin S, Italiano A. CSF-1R Inhibitor Development: Current Clinical Status. Curr Oncol Rep 2017;19(11):70 doi 10.1007/s11912-017-0634-1. [PubMed: 28875266]
15. Tap WD, Wainberg ZA, Anthony SP, Ibrahim PN, Zhang C, Healey JH, et al. Structure-Guided Blockade of CSF1R Kinase in Tenosynovial Giant-Cell Tumor. N Engl J Med 2015;373(5):428–37 doi 10.1056/NEJMoa1411366. [PubMed: 26222558]
16. Tap WD, Gelderblom H, Palmerini E, Desai J, Bauer S, Blay J-Y, et al. Pexidartinib versus placebo for advanced tenosynovial giant cell tumour (ENLIVEN): a randomised phase 3 trial. The Lancet 2019;394(10197):478–87 doi 10.1016/s0140-6736(19)30764-0.
17. Lamb YN. Pexidartinib: First Approval. Drugs 2019;79(16):1805–12 doi 10.1007/s40265-019-01210-0. [PubMed: 31602563]
18. Cannarile MA, Weisser M, Jacob W, Jegg AM, Ries CH, Ruttinger D. Colony-stimulating factor 1 receptor (CSF1R) inhibitors in cancer therapy. J Immunother Cancer 2017;5(1):53 doi 10.1186/s40425-017-0257-y. [PubMed: 28716061]
19. Wesolowski R, Sharma N, Reebel L, Rodal MB, Peck A, West BL, et al. Phase Ib study of the combination of pexidartinib (PLX3397), a CSF-1R inhibitor, and paclitaxel in patients with advanced solid tumors. Ther Adv Med Oncol 2019;11:1758835919854238 doi 10.1177/1758835919854238. [PubMed: 31258629]
20. Patwardhan PP, Surriga O, Beckman MJ, de Stanchina E, Dematteo RP, Tap WD, et al. Sustained inhibition of receptor tyrosine kinases and macrophage depletion by PLX3397 and rapamycin as a potential new approach for the treatment of MPNSTs. Clin Cancer Res 2014;20(12):3146–58 doi 10.1158/1078-0432.CCR-13-2576. [PubMed: 24718867]
21. Asai T, Ueda T, Itoh K, Yoshioka K, Aoki Y, Mori S, et al. Establishment and characterization of a murine osteosarcoma cell line (LM8) with high metastatic potential to the lung. International journal of cancer 1998;76(3):418–22. [PubMed: 9579581]
22. Burton L, Paget D, Binder NB, Bohnert K, Nestor BJ, Sculco TP, et al. Orthopedic wear debris mediated inflammatory osteolysis is mediated in part by NALP3 inflammasome activation. J Orthop Res 2013;31(1):73–80 doi 10.1002/jor.22190. [PubMed: 22933241]
23. Takeshita S, Kaji K, Kudo A. Identification and characterization of the new osteoclast progenitor with macrophage phenotypes being able to differentiate into mature osteoclasts. J Bone Miner Res 2000;15(8):1477–88. [PubMed: 10934646]
24. Yuan J, Ossendorf C, Szatkowski JP, Bronk JT, Maran A, Yaszemski M, et al. Osteoblastic and osteolytic human osteosarcomas can be studied with a new xenograft mouse model producing spontaneous metastases. Cancer Invest 2009;27(4):435–42 doi 10.1080/07357900802491477. [PubMed: 19212826]
25. Faccio R, Takeshita S, Colaianni G, Chappel J, Zallone A, Teitelbaum SL, et al. M-CSF regulates the cytoskeleton via recruitment of a multimeric signaling complex to c-Fms Tyr-559/697/721. J Biol Chem 2007;282(26):18991–9. [PubMed: 17420256]
26. Zhang W, Xu W, Xiong S. Macrophage differentiation and polarization via phosphatidylinositol 3-kinase/Akt-ERK signaling pathway conferred by serum amyloid P component. J Immunol 2011;187(4):1764–77 doi 10.4049/jimmunol.1002315. [PubMed: 21753147]

27. Cuccarese MF, Dubach JM, Pfirschke C, Engblom C, Garris C, Miller MA, et al. Heterogeneity of macrophage infiltration and therapeutic response in lung carcinoma revealed by 3D organ imaging. Nat Commun 2017;8(1):1–10. [PubMed: 28232747]
28. De Palma M, Lewis CE. Macrophages limit chemotherapy. Nature 2011;472(7343):303–4. [PubMed: 21512566]
29. Salvagno C, Ciampricotti M, Tuit S, Hau C-S, van Weverwijk A, Coffelt SB, et al. Therapeutic targeting of macrophages enhances chemotherapy efficacy by unleashing type I interferon response. Nat Cell Biol 2019;21(4):511–21. [PubMed: 30886344]
30. Xu J, Escamilla J, Mok S, David J, Priceman S, West B, et al. CSF1R signaling blockade stanches tumor-infiltrating myeloid cells and improves the efficacy of radiotherapy in prostate cancer. Cancer Res 2013;73(9):2782–94. [PubMed: 23418320]
31. Anthony SP, Puzanov I, Lin PS, Nolop KB, West B, Hoff DDV. Pharmacodynamic activity demonstrated in phase I for PLX3397, a selective inhibitor of FMS and Kit. Journal of Clinical Oncology 2011;29(15_suppl):3093- doi 10.1200/jco.2011.29.15_suppl.3093.
32. Wainberg ZP-PS, Luke J, Kim E, Thompson J, Pfanzelter N. 32nd Annual Meeting and Pre-Conference Programs of the Society for Immunotherapy of Cancer (SITC 2017): Part One. Journal for ImmunoTherapy of Cancer 2017;5(2):86 doi 10.1186/s40425-017-0289-3.
33. Osipov A, Saung MT, Zheng L, Murphy AG. Small molecule immunomodulation: the tumor microenvironment and overcoming immune escape. J Immunother Cancer 2019;7(1):224 doi 10.1186/s40425-019-0667-0. [PubMed: 31439034]
34. Arakaki R, Yamasaki T, Kanno T, Shibasaki N, Sakamoto H, Utsunomiya N, et al. CCL 2 as a potential therapeutic target for clear cell renal cell carcinoma. Cancer Med 2016;5(10):2920–33. [PubMed: 27666332]
35. Marques P, Barry S, Carlsen E, Collier D, Ronaldson A, Awad S, et al. Chemokines modulate the tumour microenvironment in pituitary neuroendocrine tumours. Acta Neuropathol Commun 2019;7(1):172 doi 10.1186/s40478-019-0830-3. [PubMed: 31703742]
36. Xuan W, Qu Q, Zheng B, Xiong S, Fan GH. The chemotaxis of M1 and M2 macrophages is regulated by different chemokines. J Leukoc Biol 2015;97(1):61–9 doi 10.1189/jlb.1A0314-170R. [PubMed: 25359998]
37. Li Y, Zheng Y, Li T, Wang Q, Qian J, Lu Y, et al. Chemokines CCL2, 3, 14 stimulate macrophage bone marrow homing, proliferation, and polarization in multiple myeloma. Oncotarget 2015;6(27):24218. [PubMed: 26155942]
38. Miller MA, Zheng YR, Gadde S, Pfirschke C, Zope H, Engblom C, et al. Tumour-associated macrophages act as a slow-release reservoir of nano-therapeutic Pt(IV) pro-drug. Nat Commun 2015;6:8692 doi 10.1038/ncomms9692. [PubMed: 26503691]
39. Sun W, Wei FQ, Li WJ, Wei JW, Zhong H, Wen YH, et al. A positive-feedback loop between tumour infiltrating activated Treg cells and type 2-skewed macrophages is essential for progression of laryngeal squamous cell carcinoma. Br J Cancer 2017;117(11):1631–43 doi 10.1038/bjc.2017.329. [PubMed: 28949956]
40. Peranzoni E, Lemoine J, Vimeux L, Feuillet V, Barrin S, Kantari-Mimoun C, et al. Macrophages impede CD8 T cells from reaching tumor cells and limit the efficacy of anti-PD-1 treatment. Proc Natl Acad Sci U S A 2018;115(17):E4041–E50 doi 10.1073/pnas.1720948115. [PubMed: 29632196]
41. Franklin RA, Liao W, Sarkar A, Kim MV, Bivona MR, Liu K, et al. The cellular and molecular origin of tumor-associated macrophages. Science 2014;344(6186):921–5. [PubMed: 24812208]
42. Mikucki M, Fisher D, Matsuzaki J, Skitzki J, Gaulin N, Muhitch J, et al. Non-redundant requirement for CXCR3 signalling during tumoricidal T-cell trafficking across tumour vascular checkpoints. Nat Commun 2015;6(1):1–14.
43. Neubert NJ, Schmittnaegel M, Bordry N, Nassiri S, Wald N, Martignier C, et al. T cell–induced CSF1 promotes melanoma resistance to PD1 blockade. Sci Transl Med 2018;10(436):eaan3311. [PubMed: 29643229]

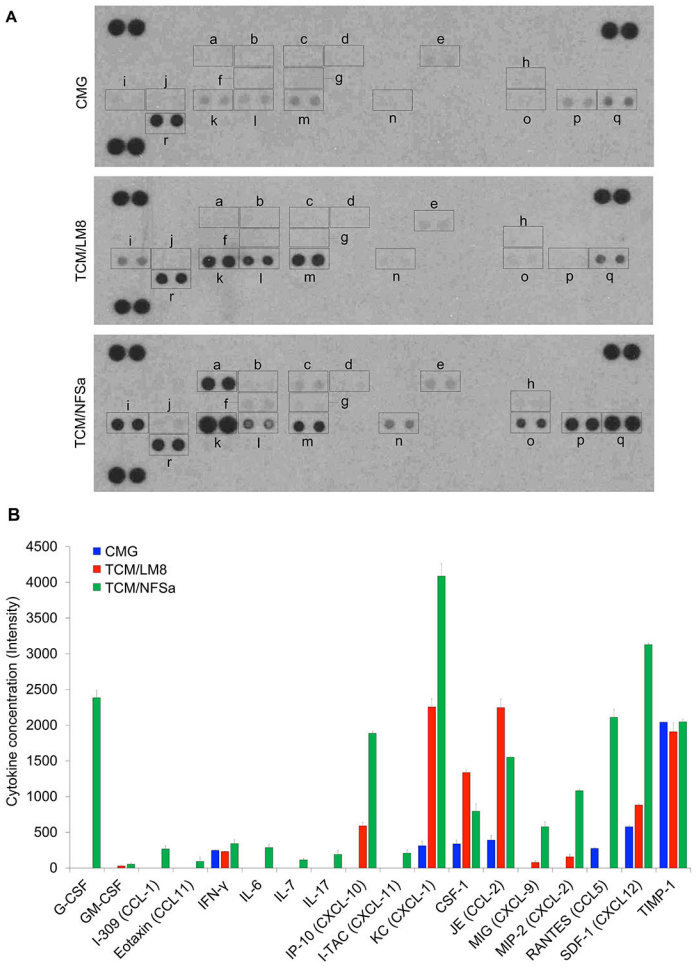

Figure 1.

Profiling of cytokine/chemokine produced from CMG, LM8, and NFSa cell lines.

A. Cytokine/chemokine production in the culture supernatant tested by cytokine array. a. G-CSF; b., GM-CSF; c. I-309 (CCL-1); d. Eotaxin (CCL11); e. IFN-γ; f. IL-6; g. IL-7; h. IL-17; i. IP-10 (CXCL-10); j. I-TAC (CXCL-11); k. KC (CXCL-1); l. CSF-1; m. JE (CCL-2); n. MIG (CXCL-9); o. MIP-2 (CXCL-2); p. RANTES (CCL5); q. SDF-1 (CXCL12); r. TIMP-1. B. Concentration of cytokines/chemokines in CMG, TCM/LM8, and TCM/NFSa, evaluated by the signal intensity shown in A.

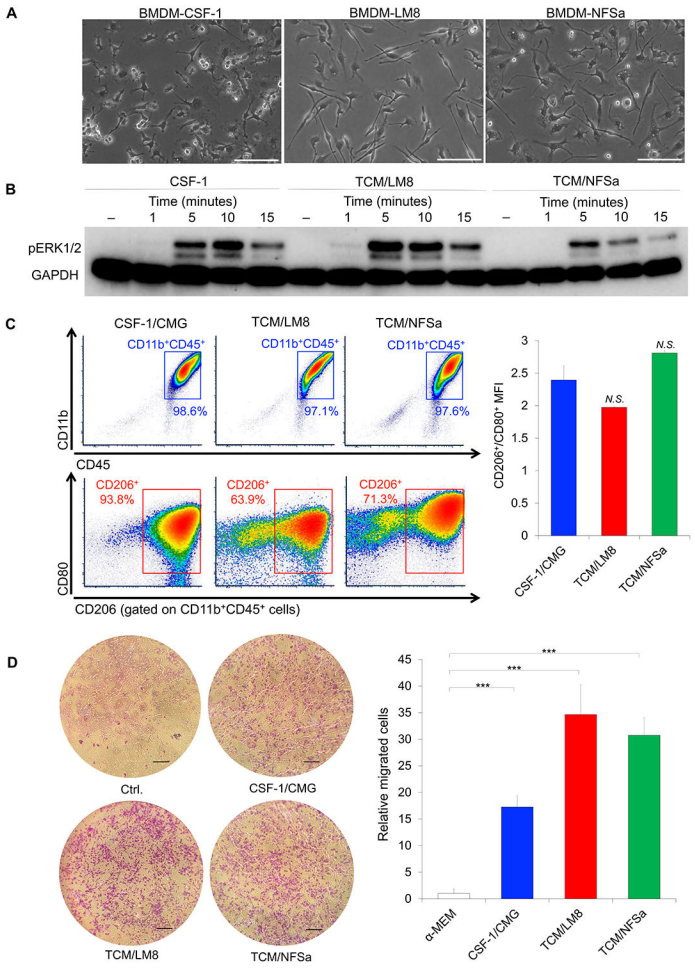

Figure 2.

Cellular features of TAMs produced by culture supernatant of bone and soft tissue sarcoma cells.

A. Morphology of BMDM-TAMs after expansion of BMDMs with culture supernatant of CMG, LM8, and NFSa cell lines. Bars, 100 μm. B. Western blots showing pERK/2 levels in BMDM-TAMs with M-CSF, TCM/LM8, and TCM/NFSa at the time points indicated. Enhanced pERK1/2 was detected with a peak stimulation after five, 10, and 15 minutes, respectively. C. Surface marker profile of BMDM-TAMs produced by CSF-1/CMG, TCM/LM8, and TCM/NFSa, assessed by flow cytometry. Right, cellular distribution of $CD45^+/CD11b^+$ and $CD45^+CD11b^+CD206^+/CD45^+CD11b^+CD80^+$. Left, the MFI of $CD206^+/CD80^+$. N.S., not significant. D. Trans-well assay to evaluate the chemotaxis of BMDMs in response to M-CSF, TCM/LM8, and TCM/NFSa. Left, photographs of BMDMs passed through the trans-well chamber. Scale bar, 200 μm. Right, the numbers of BMDMs passed through the trans-well chamber. Data are presented as mean ± SD ($n = 3$ per group). ***$p < 0.001$, Mann-Whitney U test.

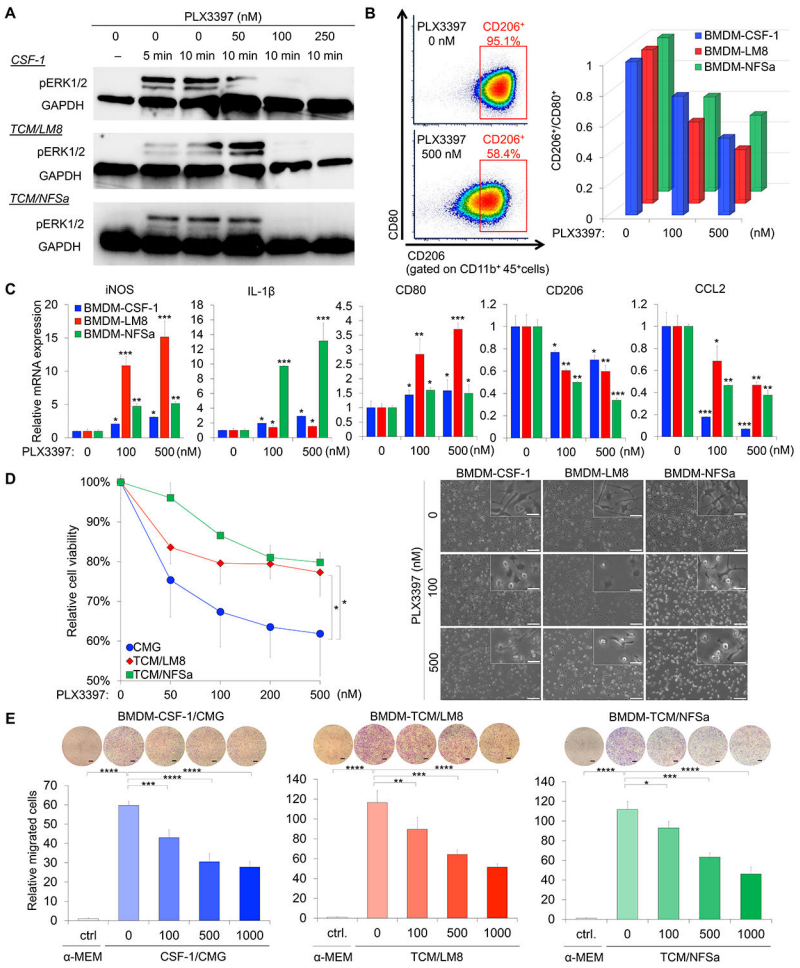

Figure 3.

CSF-1R inhibition reduces M2 polarization and deplete tumor-associated macrophages in bone and soft-tissue sarcoma model. A. Eradication of pERK1/2, stimulated with M-CSF, TCM/LM8, and TCM/NFSa, at 100 nM and 250 nM of PLX3397. B. Depolarization of BMDM-CSF-1, BMDM-LM8, and BMDM-NFSa against M2-like phenotype. Upper, decreased percentage of $CD45^+/CD11b^+/CD206^+$ populations by PLX3397 treatment (0 nM, 100 nM, and 500 nM). Lower, decreased MFI of $CD206^+/CD80^+$ by PLX3397 treatment (0 nM, 100 nM, and 500 nM). C. Quantification of mRNA expression of M1 and M2 genes, including IL-1β, iNOS, CD80, CD206, and CCL-2, after PLX3397 treatment (0 nM, 100 nM, and 500 nM). HPRT was uses as an internal control. Data are presented as mean ± SD (n = 3 per group). D. Survival of TAMs in response to PLX3397 treatment. Right, phase-contrast micrograph of BMDMs in the presence of 100 nmol/l and 500 nmol/l PLX3397. Scale bar, 100 μm (lower) and 25 μm (upper). Light, relative proliferation rates of BMDM-CSF-1, BMDM-LM8, and BMDM-NFSa after 24 hour treatment with increasing dose of PLX33897 (0, 50, 100, 200, and 500 nM). Data are presented as mean ± SD ($n = 3$ per group). *$p < 0.05$, ***$p < 0.001$; one-way analysis of variance with Sidak's multiple comparisons test. E. Trans-well chemotaxis. Macrophage migration was reduced by PLX3397 in a dose-dependent manner (0, 100, 500, 1000 nmol/l). At the time periods of one-hour post-treatment, cells were seeded and cultured on the trans-well chamber for six

hours. The number of migrated cells were photographed (upper) and counted (lower). Scale bar, 200 μm. *$p < 0.05$, **$p < 0.01$, ***$p < 0.001$, ****$p < 0.0001$; Student's *t*-test.

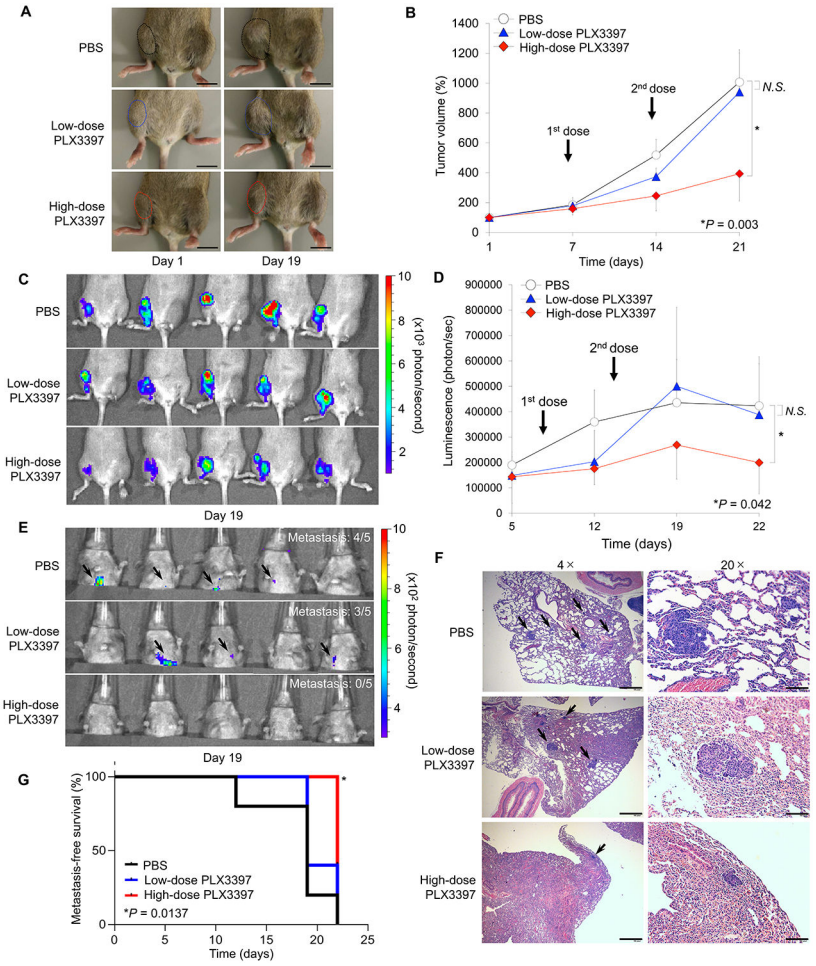

Figure 4.

CSF-1R inhibition by PLX3397 blocks tumor growth and improves metastasis-free survival in orthotopic osteosarcoma mouse model. A. Macroscopic appearance of LM8-Luc tumors in C3H/JeJ mice on Days 0 and 19 after tumor cell inoculation. Mice were inoculated intratibially with LM8-Luc cells (1×10^6 cells/site) and were systemically treated with control PBS, low-dose PLX3397 (5 mg/kg), or high-dose PLX3397 (10 mg/kg) on Day seven and 14. Tumor masses are outlined by a dotted line. B. Tumor growth in an orthotopic LM8 osteosarcoma xenograft model of each treatment group ($n = 5$ per group). Data was expressed as mean tumor volume ± SD. *$p < 0.05$, as compared with high-dose PLX3397 and PBS group; one-way ANOVA corrected for multiple comparisons. C. Luminescence intensity from the primary tumors of each treatment group measured on Day 19 using an IVIS. D. Monitoring of luminescence intensity from the primary tumors of each treatment group. Data was expressed as mean tumor volume ± SD. *$p < 0.05$, as compared with high-dose PLX3397 and PBS group; one-way ANOVA corrected for multiple comparisons. E. Lung metastases measured on Day 19 using an IVIS. F. Lung metastases validated by H&E staining. Black arrow represents metastatic foci in the lung. Scale bar, 200 μm (left). Scale bar, 40 μm (right). G. Kaplan-Meier curves showing metastasis-free survival for each group of mice. Log-rank test was performed between PBS control group (black line) and

low-dose PLX3397 group (blue line; $p = 0.353$) or high-dose PLX3397 group (red line; $*p = 0.0014$).

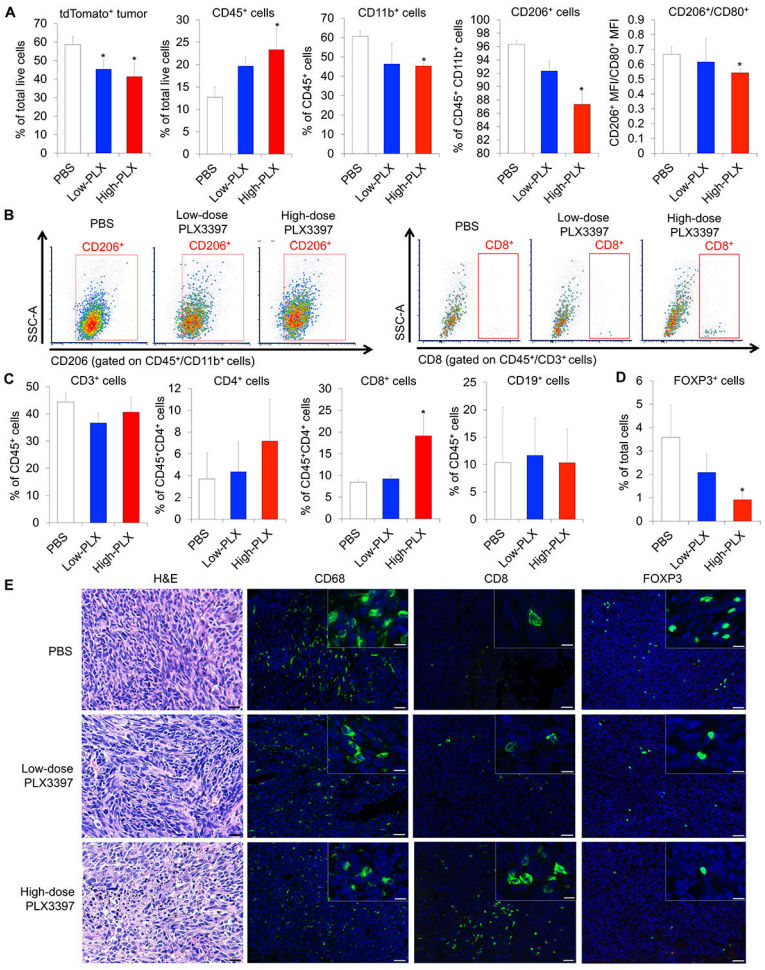

Figure 5.

Systemic treatment of PLX3397 depletes TAMs and increases lymphocyte infiltration into LM8 osteosarcoma. A. Composition of tumor cells and TAMs evaluated by flow-cytometric analysis using the dissociated LM8 tumor cells. Data were represented as mean ± SEM; $n = 3$; Mann–Whitney test: $*p < 0.05$. B. Flow cytometry analysis of TAMs ($CD45^+CD11b^+CD206^+$; left) and CD8 T cells ($CD45^+CD3^+CD8^+$; right) within the dissociated LM8 tumor cells and representative flow data. C. Composition of infiltrating immune cells ($CD3^+$, $CD4^+$, and $CD8^+$ cells) evaluated by flow-cytometric analysis using the dissociated LM8 tumor cells. Data were represented as mean ± SEM; $n = 3$; Mann – Whitney test: $*p < 0.05$. D. Composition of infiltrating $FOXP3^+$ regulatory T cells evaluated by immunohistochemistry using the dissociated LM8 tumor cells. Data were represented as mean ± SEM; $n = 3$; Mann–Whitney test: $*p < 0.05$. E. Distribution of infiltrating $CD68^+$ macrophages, $CD8^+$ T cells, and $FOXP3^+$ regulatory T cells in PLX3397- or PBS-treated tumors (green). Nuclei were stained with DAPI (blue). Left, H&E staining images. Scale bars, 50 μm (lower) and 10 μm (upper).